P4.22

EFFECTS OF LANDFALL LOCATION AND THE APPROACH ANGLE OF A CYCLONE ENCOUNTERING A MESOSCALE MOUNTAIN RANGE

Yuh-Lang Lin*, L. Crosby Savage III, and Christopher M. Hill
Department of Marine, Earth, and Atmospheric Sciences
North Carolina State University, Raleigh, North Carolina

1. INTRODUCTION

As a cyclone passes over a mesoscale mountain range, its track is often deflected by a mountain range (Lin et al. 1999), as occurs with typhoons passing over the Central Mountain Range (CMR) of Taiwan or the Cordillera Central of northern Luzon in the Philippines (Wang 1980, Bender et al. 1987), with hurricanes passing over the Cordillera Central of Hispañola (Bender et al. 1987) and the Sierra Madre Mountains of Mexico (Zehnder 1993; Zehnder and Reeder 1997), and with cyclones passing over the Appalachians (O'Handley and Bosart 1996) and over Greenland (Schwierz and Davies 2003). Because it is a steep mountain range isolated by significant bodies of water, and is often traversed by western Pacific TCs, the CMR has been studied extensively for its orographic influence on TC track continuity and deflection.

Lin et al. (2005) identified six prospective non-dimensional control parameters for diagnosing the continuity and deflection of cyclone tracks across a mesoscale mountain range. From previous studies of observed and simulated typhoons traversing the CMR, and from idealized simulations of a westward-moving cyclone over idealized CMR, it has been found that the cyclone track is discontinuous (continuous), and the cyclone encounters more (less) deflection in its motion, with a combination of small (large) values of the parameters V_{max}/Nh, U/Nh, R/L_y, U/fL_x, and V_{max}/fR, and a large (small) value of the parameter h/L_x. The symbols comprising the parameters are defined as: V_{max}, the maximum tangential wind; N, the Brunt-Väisäla frequency; h, the mountain height; U, the basic wind speed; R, the radius of V_{max}; f, the Coriolis parameter; L_x and L_y, the horizontal scales of the mountain in x and y directions, respectively. In particular, the first three parameters were found to play a dominant role in controlling the deflection of cyclone tracks for typhoons passing over the CMR. The left or right track deflection appears to be controlled more by V_{max}/Nh and R/L_y, while the degree of track deflection is controlled more by U/Nh. In general, track deflection is controlled by the dynamics of orographic blocking.

In addition to the above-listed control parameters, the deflection in the track of a tropical cyclone traversing the CMR is also strongly influenced by the landfall location and approach angle (e.g. Wang 1980; Yeh and Elsberry 1993a,b). In this study, we plan to investigate these effects by performing idealized numerical simulations with a drifting cyclone passing over idealized topography representative of the CMR.

* *Corresponding author address*: Dr. Yuh-Lang Lin, Dept. of MEAS, North Carolina State Univ., Campus Box 8208, Raleigh, NC 27695-8208.
E-mail: yl_lin@ncsu.edu

2. MODEL DESCRIPTION AND EXPERIMENT DESIGN

We employ a mesoscale numerical model (NCSU-GFDM) to help understand the dynamics involved with different landfall locations and approach angles that affect the track of a cyclone over an idealized, mesoscale mountain range. The model has been adopted in previous studies for idealized tropical cyclones passing over mesoscale mountain ranges (e.g. Lin et al. 1999; 2005). The major characteristics of the model are summarized as follows:

- The time-dependent, hydrostatic governing equations are solved on an Arakawa-C staggered grid.
- The third-order Adams-Bashforth scheme for time marching.
- The horizontal (vertical) advection terms are approximated using quadratic conservative fourth- (second-) order-centered finite difference.
- A terrain-following (σ_z) vertical coordinate is adopted, where σ is defined as $\sigma = z_T\,(z - h) / (z_T - h)$. Here z_T and h are the heights of the computational domain and terrain elevation, respectively.
- A free-slip lower-boundary condition.
- A radiation upper-boundary condition.
- The horizontal domain average is subtracted from perturbation pressure fields in every grid point at every time step.
- A five-point numerical smoother for diffusion.
- Latent heating is excluded in all simulations.

Details of the numerical formulation of the model can be found in Lin et al. (1999).

For most cases presented here, a uniform, stably stratified basic flow is introduced instantaneously and throughout the grid domain at non-dimensional time t = 0. The Brunt-Väisäla frequency is set as $N = 0.01\ s^{-1}$ for all experiments performed in this study. An f-plane approximation has also been made, where the Coriolis parameter f_o is taken to be $5.8\times10^{-5}\ s^{-1}$. The flow is inviscid throughout the entire model domain. The vertical grid interval is 500 m, while the horizontal grid interval is $\Delta x = \Delta y = 20$ km. The numbers of grid points over the x-, y-, and z- axes are 101x81x31 for a domain size of 2000 km x 1600 km x 15 km. The CMR is idealized by a bell-shaped function as:

$$h(x,y) = \frac{h}{\left[(x/a)^2 + (y/b)^2 + 1\right]^{3/2}}, \qquad (1)$$

where h is the mountain height, and a and b are the mountain half-widths in the x- and y-directions, respectively. For all cases performed in this study, we

use h = 2.5 km, a = 40 km and b = 120 km, which are values comparable to those attributed to the CMR. Note that we use 2a and 2b to roughly represent L_x and L_y, respectively.

Identical to Lin et al. (2005), an idealized tropical cyclone is initialized with a prescribed tangential velocity following Chang (1982) and Huang and Lin (1997):

$$v_\theta = v_{\max}\left(\frac{r}{R_{\max}}\right)\exp\left\{\frac{1}{2}\left[1-\left(\frac{r}{R_{\max}}\right)^2\right]\right\}, \quad (2)$$

where v_{max} is the maximum tangential velocity at a radius of R_{max} from the cyclone center. The details of the model initialization procedure can be found in Lin et al. (1999). As latent heating effects were not used in this study, simulated cyclone vortices were prescribed with relatively large radii of maximum wind (R) to ensure barotropic stability with the simulated vortex.

This problem is studied by performing systematic numerical modeling simulations using a simple mesoscale model. The control parameters are fixed with U / Nh = 0.4, V_{max} / Nh = 0.8, and R / L_y = 0.75. The control case (Case E) has the cyclone approaching the idealized mountain range from a point 500 km east of the mountain range center, or from (x/a, y/a) = (12.5, 0.0). The effect of landfall location is then studied through two additional cases: Case N, in which the cyclone is approaching the mountain range from the east with (x/a, y/a) = (12.5, 2.25); and Case S, in which the cyclone is approaching from the east with (x/a, y/a) = (12.5, -2.25). The effect of approach angle is studied through two more cases, each in which the cyclone encounters the mountain range at a central-east location with (x/a, y/a) = (1.0, 0.0). In Case NE, the cyclone approaches the mountain range starting from (x/a, y/a) = (8.133, 8.132); in Case SE, the cyclone approaches the mountain range from (x/a, y/a) = (8.133, -8.132). The effects of both approach angle and landfall location are studied through four more cases, each in which encounter the mountain range at a northeast location with (x/a, y/a) = (0.0, 2.25) or a southeast location with (x/a, y/a) = (0.0, -2.25). In Case NE-N, the cyclone is approaching from (x/a, y/a) = (8.133, 10.381) and encounters the mountain range at (x/a, y/a) = (0.0, 2.25); in Case NE-S, the cyclone is approaching from (x/a, y/a) = (8.133, 5.881) and encounters the mountain range at (x/a, y/a) = (0.0, -2.25). Case SE-S approaches the mountain range from (x/a, y/a) = (8.133, -10.381) and encounters the mountain at (x/a, y/a) = (0.0, -2.25), while Case SE-N approaches the mountain range from (x/a, y/a) = (8.133, -5.881) and encounters the mountain at (x/a, y/a) = (0.0, 2.25).

3. RESULTS

3.1. Effects of Landfall Location

Figure 1a shows the tracks of the cyclone vorticity centers at the surface and 500 mb for Case E. At the surface, the cyclone is deflected slightly to the north before it encounters the mountain, slightly to the south as it is crossing over the mountain, and to the north after crosses the mountain, and then returns to its original westward track far downstream (to the west) of the mountain. The track is less affected by the mountain at 500 mb. The surface relative vorticity fields at t = 9, 12, 15, and 18 are shown in Figs. 2a-d, respectively. At t = 9 h (Fig. 2a), the vorticity center is located at about (x/a, y/a) = (10.0, 0.0), indicative of no deflection in cyclone motion. A weak vorticity center forms on the lee side at this time. Before the cyclone encounters the mountain at t = 12h (Fig. 2b), the upstream vorticity pattern is distorted slightly toward north and the track of the vorticity center is deflected slight to the north. At 15 h (Fig. 2c), the lee side vorticity center becomes the cyclone center, with a resulting discontinuity in the track (Fig. 1a). At 18 h (Fig. 2d), the cyclone is deflected to the north and resumes its original westward direction afterwards.

Deflection to the surface track of the cyclone approaching from the east can be explained through a vorticity budget analysis, in which individual terms of the vorticity equation,

$$\frac{\partial\zeta}{\partial t} = -\vec{V}\cdot\nabla\zeta + (\zeta + f_0)\left(\frac{\partial u}{\partial x}+\frac{\partial v}{\partial y}\right)+\left(\xi\frac{\partial w}{\partial x}+\eta\frac{\partial w}{\partial y}\right)+R \quad (3)$$

are calculated. In Eq. (3), ξ, η, and ζ represent vorticity in the x-, y-, and z-directions, respectively. The term on the left side is the local rate of change of the vertical relative vorticity or local vorticity generation. The terms on the right side represent, from left to right, vorticity advection, vorticity stretching, vorticity tilting, and the combined effects of turbulent mixing and numerical diffusion. Since the fluid is assumed to be Boussinesq, no solenoidal term is included in the vorticity equation. Figure 3a shows the local rate of change of the vertical vorticity at 9 h. The major area for local vorticity generation is located to the southwest of the mountain range, and a minor area is located near the east edge of the mountain range (Fig. 3a) and is mainly a product of vorticity advection and slightly contributed by the vorticity stretching for the lee side maximum area (Figs. 3b and 3c). Since the upstream local vorticity generation maximum is centered at y/a = 0, the track of vorticity center runs straight westward. At 12 h (Fig. 4), the maximum area of local vorticity generation is located over the lee side, which is a result of vorticity stretching to the west and of the vorticity advection to the southwest. At this time, the maximum of vorticity advection (Fig. 4b) is still located upstream of the mountain range. The vorticity center is located slightly to the north of the y/a = 0 line, indicative of a slight northward deflection in the vorticity track. After the cyclone has passed over the mountain (Figs. 5 and 6), the cyclone track is shaped primarily by vorticity advection.

Figure 7 shows the vorticity fields at t = 9, 12, 15, and 18 h for case N. The vorticity center is deflected slightly northward of its original east-west track before encountering the mountain range. The cyclone is deflected to the south during its passage over the

mountain range, to the north on the lee side of the mountain range, and then resumes westward movement far downstream (Fig. 1b). Based on the vorticity budget analysis (not shown), the slight upstream northward deflection is due to vorticity advection, while the southward deflection during its passage over the mountain is dominated by the vorticity stretching. The resumption of westward motion is controlled by vorticity advection. Figure 8 shows the vorticity fields at t = 9, 12, 15, and 18 h for case S. The vorticity center curves clockwise around the southern part of the mountain range, overshoots to the north on the lee side, and then resumes westward movement far downstream (Fig. 1c). Based on the vorticity budget analysis (not shown), the upstream southward deflection is due to vorticity advection as the cyclone approaches the mountain. Around t = 15 h, the northward deflection on the lee side is dominated by vorticity stretching. Far downstream of the mountain range, the cyclone resumes westward movement due to vorticity advection.

3.2. Effects of Approach Angle

For cyclone landfall at the east-central part of the mountain range from the northeast (Case NE), the cyclone (vorticity) center is almost unaffected by the mountain upstream; it deviates to the right after passing the peak of the mountain range (Fig. 1d; Fig. 9). The vorticity center then turns cyclonically and resumes southwestward movement far downstream. At t = 9 h, a region of strong (weak) vorticity advection is produced over the northern (southern) portion of the mountain, mainly due to the flow splitting at the east-central landfall location. These two maximum regions of vorticity advection are enhanced by a dipole configuration of vorticity stretching; in which positive vorticity is generated to the north of the mountain range and negative vorticity is generated to the south. A resulting dipole pattern of local vorticity generation is oriented southeast to northwest, canceling any effect on cyclone motion at this hour. At t = 12 h, the combined effect of vorticity advection and vorticity stretching shifts the dipole of local vorticity generation pattern to a northeast-southwest configuration (not shown). Since it aligned in the same direction as the cyclone movement, the track deflection is again very small. Around t = 15 h, the local rate of change of vorticity is dominated by the vorticity stretching term, which has a maximum over the west-central portion of the mountain range. The vorticity center is, therefore, deflected to the right on the lee side near the mountain (Fig. 1d). At t = 18 h, the vortex resumes its original southwestward movement, which is controlled by vorticity advection.

For cyclone landfall from the southeast (Case SE), the track deflection of the surface cyclone (vorticity) center is quite different from that of Case NE (Fig. 1e; Fig. 10). The vorticity center is deflected to the right upstream of the mountain peak and to the left downstream of the mountain peak, but resumes its northwestward movement far downstream. The rightward deflection of the vorticity center upstream is mainly due to vorticity advection, while the leftward deflection downstream is influenced mainly by vorticity stretching.

3.3. Effects of Landfall Location and Approach Angle

Figure 11a shows the vorticity tracks of Case NE-N, which, unlike Case NE, is affected by the mountain upstream causing a deflection to the left. This leftward deflection is mainly influenced by vorticity stretching. At t = 18 h, the flow splits with two regions of maximum vorticity oriented NW and SE around the mountain range. The split flow is caused by an increase in vorticity stretching on the lee side of the mountain, and at t = 21 h, the lee side vorticity stretching becomes dominant creating a rightward deflection. At t = 27 h, vorticity advection controls the cyclone, which resumes its southwestward movement. For cyclone landfall at the southern part of the mountain range from the northeast (Case NE-S), the vorticity center follows a similar path to Case NE. Just like Case NE, a region of strong vorticity advection forms near the east-central part of the mountain and is enhanced by a north south dipole configuration of vorticity stretching. Again a dipole pattern of local vorticity cancels any influence on cyclone motion. At t = 15 h, the vorticity center is deflected to the right on the lee side near the mountain due to an increase in vorticity stretching (Fig. 11b). The cyclone then returns to its original track as vorticity advection takes control.

Figure 11c shows the vorticity tracks of Case SE-S. Upwind of the mountain range the cyclone is deflected to the left by a strong region of vorticity advection. At t = 12 h, the flow splits into two regions of maximum vorticity; in which one center is located to the south of the mountain and the other center is located to the west of the mountain. The southern center of maximum vorticity is controlled by vorticity advection, while the western center is dominated by vorticity stretching. At t = 15 h, the western center dissipates due to strong negative vorticity advection, while the southern center remains deflected to the left, but is now influenced by vorticity stretching. At t = 21 h, the cyclone center resumes its northwestward movement, which is controlled by vorticity advection. For cyclone landfall at the northern part of the mountain range from the southeast (Case SE-N), the vorticity center follows a similar path to Case SE. Upstream of the mountain the center is deflected to the right by vorticity advection (Fig. 11d). At t = 12 h, a second vorticity center develops on the lee side from vorticity stretching and has a leftward deflection. This vorticity max becomes dominant at t =15 h, and moves directly northward from both vorticity stretching and advection. The cyclone then resumes its original track and is mainly controlled by vorticity advection.

4. SUMMARY

In summary, the deflection of a cyclone encountering a mountain range is largely controlled by vorticity advection and stretching, depending upon the landfall location and approach angle of the cyclone.

Generally speaking, the local vorticity generation is dominated more by vorticity advection upstream of the mountain range, and by vorticity stretching downstream and near the mountain range. Far downstream of the mountain, the local vorticity generation is again dominated by the vorticity advection, as it steers the vortex back to its original direction of movement.

Acknowledgments: The authors would like to thank S.-T. Wang and C.-Y. Huang for their valuable discussions. This study is partially supported by ONR Grant N00014-02-1-0674.

5. References

Bender, M. A., R. E. Tuleya, and Y. Kurihara, 1987: A numerical study of the effect of an island terrain on tropical cyclones. *Mon. Wea. Rev*., **115**, 130-155.

Chang, S. W.-J., 1982: The orographic effects induced by an island mountain range on propagating tropical cyclones. *Mon. Wea. Rev*., **110**, 1255-1270.

Huang, C.-Y., and Y.-L. Lin, 1997: The evolution of a mesoscale vortex impinging on symmetric topography. *Proc. National Science Council* (Taiwan), Part A, **21**, 285-309.

Lin, Y.-L., J. Han, D. W. Hamilton, and C.-Y. Huang, 1999 (LHHH): Orographic influence on a drifting cyclone. *J. Atmos. Sci*., **56**, 534-562.

Lin, Y.-L., S.-Y. Chen, C. M. Hill, and C.-Y. Huang, 2005: Control parameters for the influence of a mesoscale mountain range on cyclone track continuity and deflections. J. Atmos. Sci., 62, 1849-1866.

O'Handley, C., and L. F. Bosart, 1996: The impact of the Appalachian Mountains on cyclonic weather systems. Part I: A climatology. *Mon. Wea. Rev*., **124**, 1353-1373.

Schwierz, C. B., and H. C. Davies, 2003: Evolution of a synoptic-scale vortex advecting toward a high mountain. *Tellus*, **55A**, 158-172.

Wang, S.-T., 1980: Prediction of the movement and strength of typhoons in Taiwan and its vicinity, *Res. Report 108, National Science Council*, Taipei, Taiwan, 100pp.

Yeh, T.-C., and R. L. Elsberry, 1993a: Interaction of typhoons with the Taiwan topography. Part I: Upstream track deflection. *Mon. Wea. Rev*., **121**, 3193-3212.

_____, and _____, 1993b: Interaction of typhoons with the Taiwan topography. Part II: Continuous and discontinuous tracks across the island. *Mon. Wea. Rev*., **121**, 3213-3233.

Zehnder, J. A., 1993: The influence of large-scale topography on barotropic vortex motion. *J. Atmos. Sci*., **50**, 2519-2532.

_____, and M. J. Reeder, 1997: A numerical study of barotropic vortex motion near a large-scale mountain range with application to the motion of tropical cyclones approaching the Sierra Madre. *Meteor. Atmos. Phys*., **64**, 1-19.

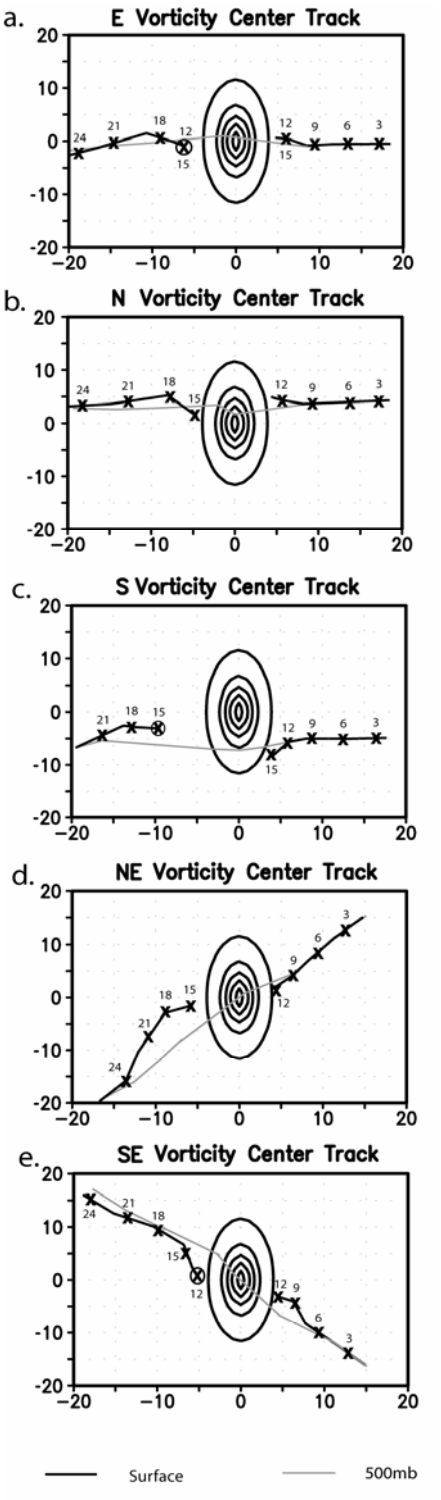

Fig. 1: Tracks of cyclone vorticity centers from GFDM near the surface and 500 mb. The X marks denote 3-hourly surface positions. A circled X denotes a second, co-existing vorticity center. Thick ovals denote terrain at every 400 m. Area shown is 800 km × 800 km.

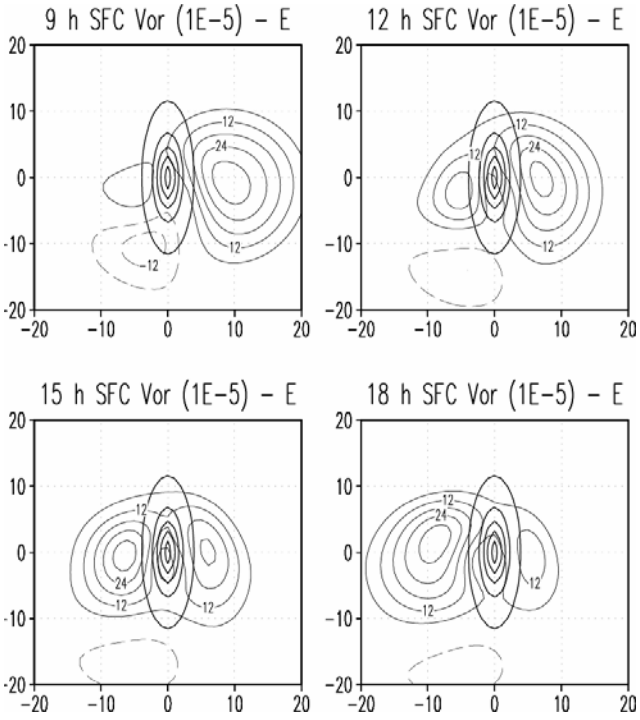

Fig. 2: GFDM vorticity, for case E, near the surface at 9, 12, 15, and 18 h. Vorticity is contoured every 6×10^{-5} s^{-1}. Solid (dashed) lines are positive (negative) values.

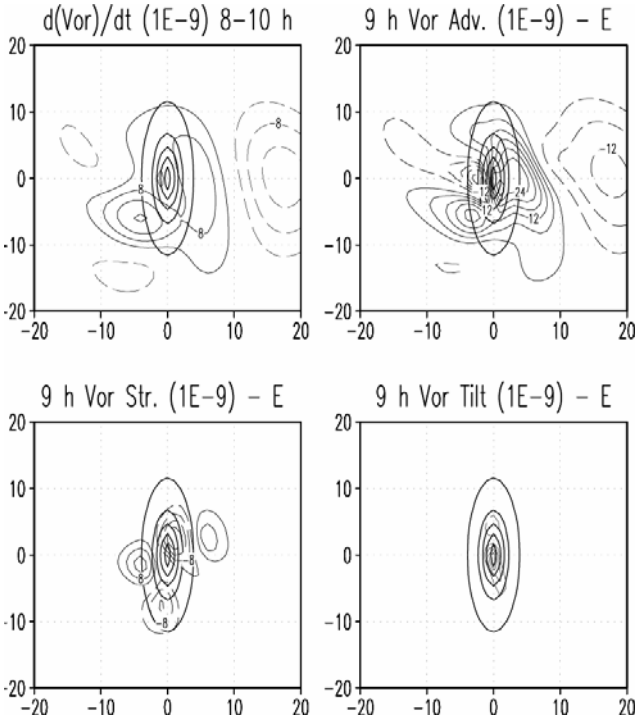

Fig. 3: Budget of GFDM vorticity terms at 9 h for Case E. Terms shown are total derivative, advection, stretching, and tilting. Contours are plotted every 4×10^{-9} s^{-2} except for advection, which is plotted every 6×10^{-9} s^{-2}.

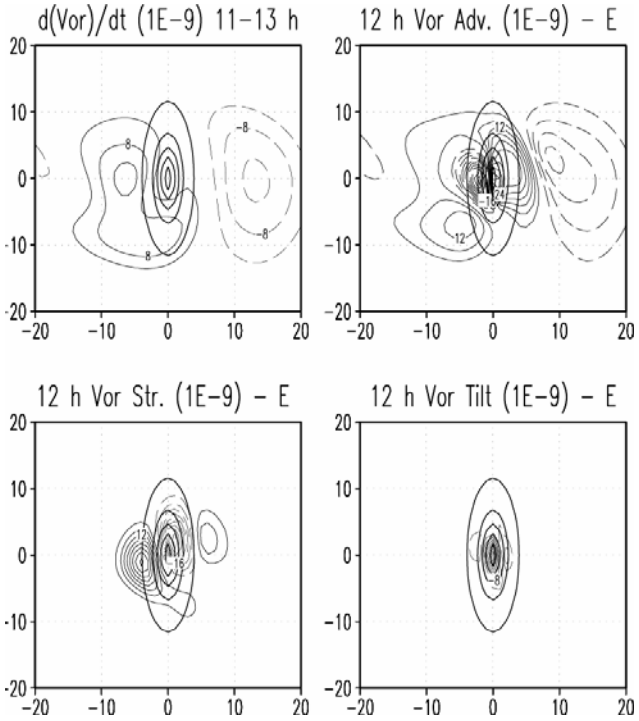

Fig. 4: Same as Fig. 3 except for 12 h.

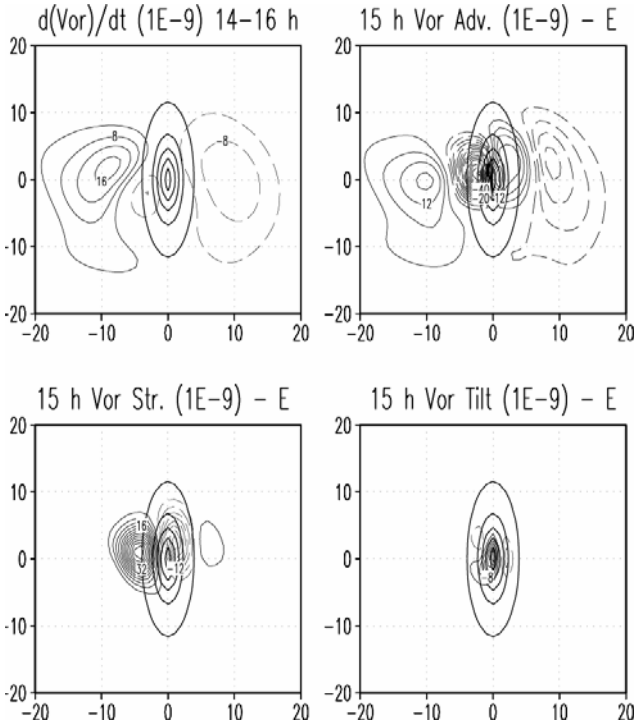

Fig. 5: Same as Fig. 3 except for 15 h.

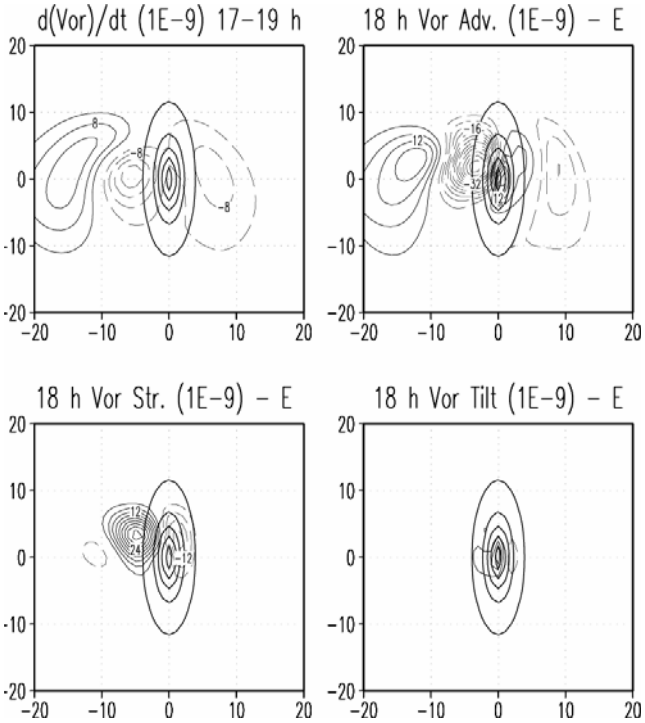

Fig. 6: Same as Fig. 3 except for 18 h.

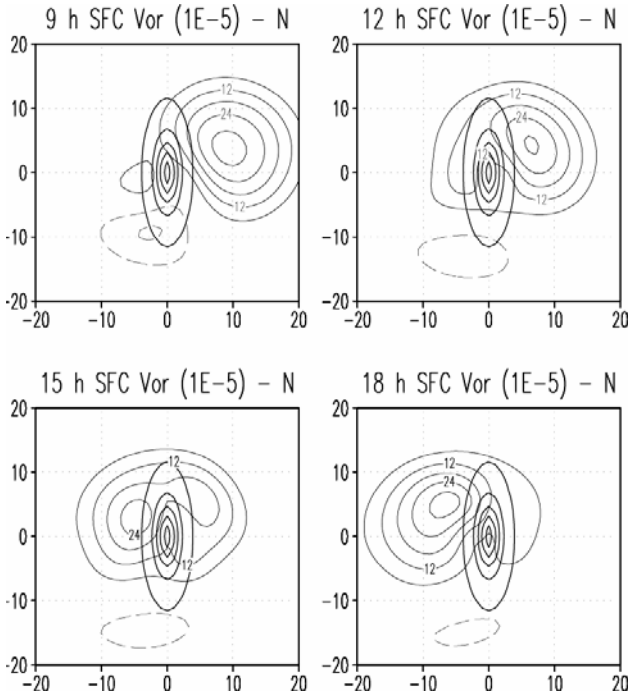

Fig. 7: Same as Fig. 2 except for case N.

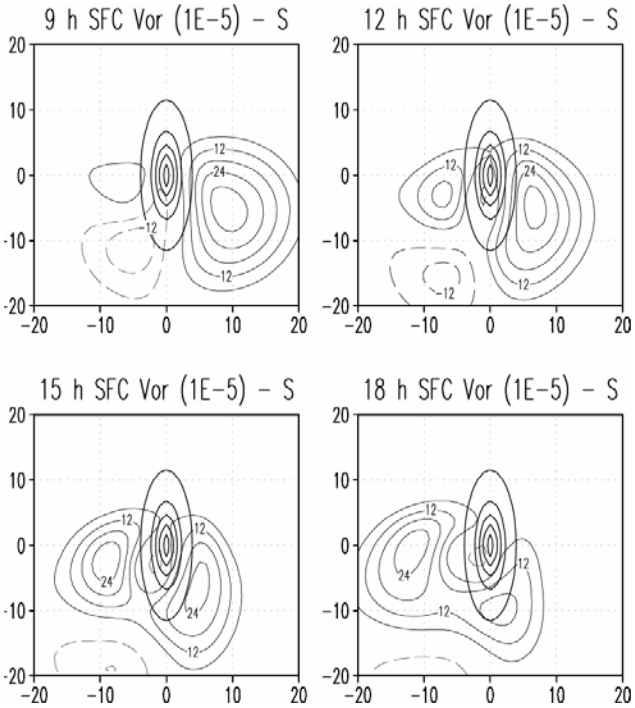

Fig. 8: Same as Fig. 2 except for Case S.

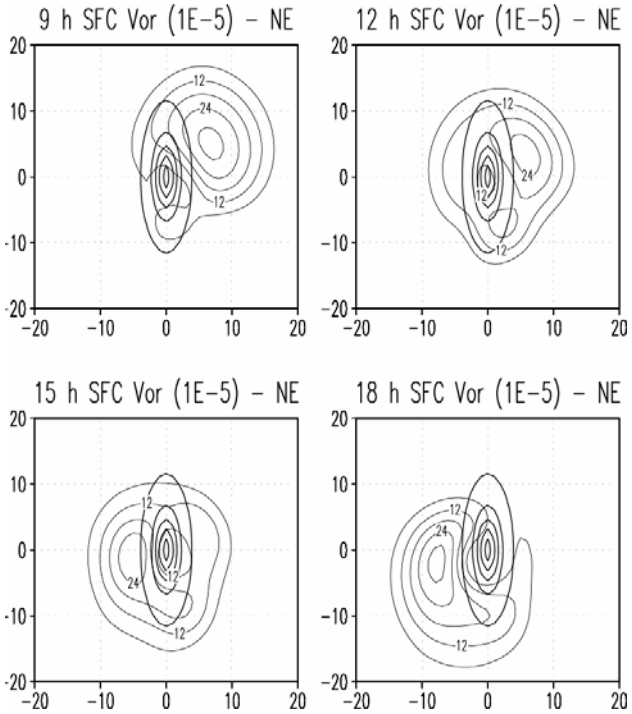

Fig. 9: Same as Fig. 2 except for Case NE.

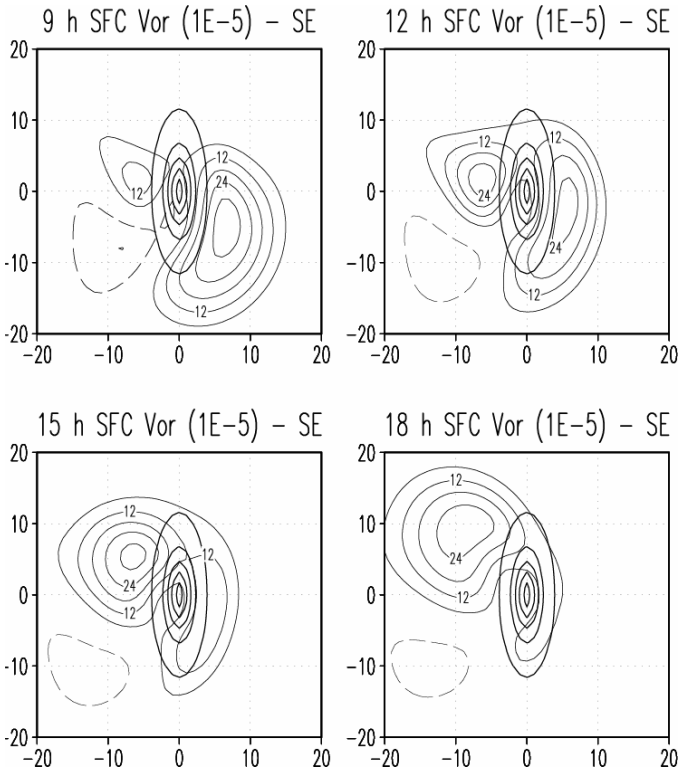

Fig. 10: Same as Fig. 2 except for Case SE.

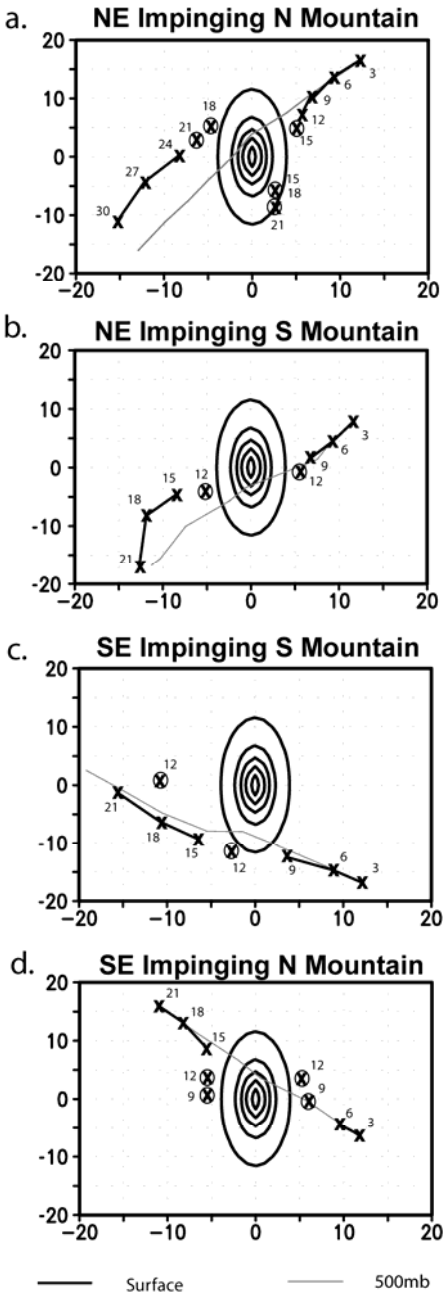

Fig. 11: Tracks of cyclone vorticity centers from GFDM near the surface and 500 mb. The X marks denote 3-hourly surface positions. A circled X denotes a second, co-existing vorticity center. Thick ovals denote terrain at every 400 m. Area shown is 800 km × 800 km.